Int J Clin Exp Med 2019;12(4):3529-3545
www.ijcem.com /ISSN:1940-5901/IJCEM0083862

Original Article

Potential mechanism of nitidine chloride in treating lipopolysaccharide-induced primary mouse bone marrow-derived dendritic cells by connectivity map and bioinformatics-based methods

Yi-Wu Dang[1], Li-Min Liu[3], Peng Lin[2], Hong Yang[2], Li-Jie Zhang[2], Gang Chen[1]

Departments of [1]Pathology, [2]Medical Ultrasonics, First Affiliated Hospital of Guangxi Medical University, Nanning, Guangxi Zhuang Autonomous Region, P. R. China; [3]Department of Toxicology, College of Pharmacy, Guangxi Medical University, Nanning, Guangxi Zhuang Autonomous Region, P. R. China

Received August 11, 2018; Accepted October 11, 2018; Epub April 15, 2019; Published April 30, 2019

Abstract: Background and objectives: Nitidine chloride, a natural bioactive phytochemical alkaloid derived from Zanthoxylum nitidum (Roxb) DC, has been an ingredient included in toothpaste in China for years. However, the detailed molecular targets and primary mechanisms of the anti-inflammatory capacity of nitidine chloride have not yet been well defined. Thus, the objective of the current study was to explore the molecules and novel potential mechanisms that modulate inflammation using modeled by lipopolysaccharide (LPS)-induced mouse bone-marrow-derived dendritic cells (BMDCs). Methods: Differentially expressed genes (DEGs) were calculated from microarrays providing gene profiles of BMDCs pre- and post-nitidine chloride treatment. The Kyoto Encyclopedia of Genes and Genomes (KEGG) pathway, gene ontology (GO) enrichment analyses and protein-protein interaction (PPI) analyses were carried out using the DAVID and STRING online databases to display the annotations for the DEGs. A connectivity map was used to further investigate similar known compounds and the potential therapeutic effects of nitidine chloride on BMDCs. Results: A total of 607 DEGs were identified from the microarray GSE102135, wherein nitidine chloride was used to treat the primary mouse LPS-stimulated BMDC cells from female wild-type C57BL/6 mice for 12 h. Post-nitidine chloride treatment on the LPS-stimulated BMDCs, the DEGs were enriched in several well-known pathways as determined from KEGG analysis. For instance, DEGs were enriched in the protein digestion and absorption and cGMP-PKG signaling pathways, which have been established to play essential parts in the inflammatory process. More importantly, phenoxybenzamine, thioguanosine, resveratrol, 8-azaguanine and irinotecan, etc., had high similarities with nitidine chloride, also exhibiting anti-inflammation properties as previously reported. Conclusions: Different key genes have been implicated in the nitidine chloride-mediated anti-inflammatory function via targeting of several key inflammatory pathways. The anti-inflammation properties of nitidine chloride were found to be mirrored by some known drugs, which helps to define the underlying mechanism of nitidine chloride treatment.

Keywords: Nitidine chloride, lipopolysaccharide, bone-marrow-derived dendritic cells (BMDCs), connectivity map

Introduction

Dendritic cells (DCs) are specialized and strong antigen-presenting cells (APCs) that play crucial roles as immune sentinels and initiators of T cell responses against infections and cancers, as well as in the occurrence of inflammation. DCs play an essential role as messengers connecting innate immunity with adaptive immunity. Consequently, DCs have been studied for application in the treatment of infections and cancers [1-4]. Moreover, DCs have been documented to function in immune regulation, such as in tolerance stimulation and autoimmunity prevention. There are two distinct functional stages for DCs: immature and mature. Immature DCs are differentiated from bone marrow progenitor cells and are present in blood or tissues that contact the external environment. These immature DCs exhibit a strong endocytic ability and a weak potency for T cell stimulation. After antigen intake, DCs can enter the stage of mature DCs. The mature DCs will then move to the secondary lymph organs to facilitate the

activation of T cells [5-9]. One pathogen-related molecule generated from DCs, lipopolysaccharide (LPS), is derived from the outer membrane of gram-negative bacteria. LPS has been reported to be a main cause of septic shock [10-15]. LPS can combine with LPS-binding protein and CD14 and subsequently bind to the Toll-like receptor 4 (TLR4) of DCs. After TLR4 is activated, DCs start the procedure of maturation [16, 17]. As DCs are vital immunomodulatory executors, the regulation of DCs activity could become a worthy method for the treatment of inflammation and autoimmune diseases. Therefore, DCs have the potential to act as pharmacological targets and novel biological modifiers of immune responses in various disorders. Bone marrow-derived mouse dendritic cells (BMDCs) are well-established cell models, as BMDCs post-activation play a pivotal role in the process of immune and inflammatory reactions [18-20].

Nitidine chloride (NC) is a natural bioactive phytochemical alkaloid which is derived from Zanthoxylum nitidum (Roxb) DC. Nitidine chloride, as an herbal ingredient, has been utilized in toothpaste in China for a long time. Recently, NC has been reported to also have favorable antioxidant, antifungal, anti-inflammatory, and analgesic bio-functions [21, 22]. Nevertheless, the accurate molecular targets and basic molecular mechanisms of its anti-inflammatory ability have not been well-defined so far.

The connectivity map (CMap) provides a web-based instrument to screen compounds for relation to a particular disease or a certain gene profile [23-27]. The use of a CMap can help identify novel, formerly unanticipated usages of known drugs. For example, nitidine chloride, whose mechanisms of action are not well understood, could be mapped with relation to the mechanisms of existing drugs. This makes the CMap a valuable instrument for augmenting the biological knowledge of a new drug.

Thus, our aim in the current study was to determine whether we can use the Cmap to detect additional molecules that modulate inflammation as modeled by LPS-induced mouse BMDCs after treatment with nitidine chloride. By doing so, we may identify a novel potential mechanism for the treatment of inflammatory diseases.

Material and methods

Publicly available data collection from GEO and ArrayExpress

To collect relative data on the differentially expressed genes influenced by nitidine chloride in BMDCs, original mRNA high-throughput RNA-sequencing or microarray profiles were gathered from the Gene Expression Omnibus (GEO) and ArrayExpress databases up to January 16th, 2018. The following literature databases were also searched: PubMed, Wiley Online Library, Web of Science, Science Direct, Cochrane Central Register of Controlled Trials, Google Scholar, EMBASE, Ovid, LILACS, Chinese CNKI, Chong Qing VIP, Wan Fang and China Biology Medicine Disc. The searching strategy contained the following keywords: “nitidine chloride” OR NC *and* BMDCs OR “bone marrow-derived mouse dendritic cells”. Studies delving into the gene profiles of BMDCs post-nitidine chloride treatment were included, and if necessary, mock controls were concurrently provided.

Data mining from RNA-sequencing or microarray profiles

The mRNA expression data were normalized and transformed by a log2 algorithm. Differential expression of mRNAs was estimated by a fold change (FC) from the comparison between experimental and control groups. Whenever the FC was greater than 2 or smaller than 0.5 as a pre-defined threshold, the corresponding mRNAs were regarded as differentially expressed genes (DEGs). Since the data processing replied on the platform of the included study, the details of the included data would be presented in the result part.

Potential mechanism of the influence of nitidine chloride on BMDCs

The potential mechanism of the influence of nitidine chloride on BMDCs was further dissected using several bioinformatics tools. The Kyoto Encyclopedia of Genes and Genomes (KEGG) pathway and gene ontology (GO) enrichment analyses were carried out using the DAVID online database to display the annotations for the identified DEGs [28-32]. The online software Panther [33-35] was also used to explore the potential interaction pathways for the influ-

ence of nitidine chloride on BMDCs. Finally, the STRING online database was used to evaluate the protein-protein interaction (PPI) network [28, 32, 36-40]. The GOplot and ggplot2 packages of R software were used to display the results of KEGG and GO analyses, respectively. The Cytoscape and ggplot2 packages of R were used to visualize the results of PPI.

Connectivity map query for DEGs post-nitidine chloride treatment

To better examine the principal prospective mechanisms of the therapeutic influences of nitidine chloride on BMDCs, the gene expression profiles of nitidine chloride treatment were applied as queries for mapping with the Connectivity Map (CMap, http://www.broadinstitute.org/cMAP/) reference database (Build 02), containing over 7,000 profiles generated from MCF7, HL60 and PC3 cells which were treated with 1,309 compounds [41-43]. A mean connectivity score and a permutation *P* value were provided for the compounds and cell lines. This score specifies the likelihood of enrichment of a set of instances within a list of all instances by chance.

Results

Eligible study with gene profiling post-nitidine chloride treatment of BMDCs

According to the searching strategy, no eligible study could be found from ArrayExpress data or literature. Nevertheless, a microarray with GEO accession (GSE102135) was included in this study. In this study, BMDCs were achieved from female wild-type C57BL/6 mice. All animal procedures were approved by the guidelines of the Institutional Animal Care and Use Committee of The Second Military Medical University, P. R. China. In brief, bone marrow was washed down from the tibiae and femurs of the mice. The red blood cells were diminished by using hypotonic lysis of 0.83% w/v ammonium chloride. On the first day of culturing, cells (10^6 cells/mL; 2 mL/well) were cultured in six-well-plate with the medium of RPMI-1640 which was supplemented with 10% v/v heat-inactivated FCS, 10 ng/mL GM-CSF and 1 ng/mL IL-4 at 37°C and 5% CO_2. On the second day, those floating cells were discarded and the remaining cells were cultured with fresh medium till the fifth day. Then, those BMDCs which were loosely adherent or not adherent at were collected for the subsequent tests. The study of GSE102135 contained four samples (GSM2728727, GSM27282728, GSM2728729 and GSM2728730), among which GSM2728729 and GSM2728730 were pre-treated with LPS to activate BMDCs. The platform of this microarray was the NimbleGen Mouse Gene Expression Array [100718_MM9_EXP] (gene-level version). The total RNA extraction was performed with TRIZOL Reagent (Cat#15596-018, Life technologies, Carlsbad, CA, US). RNA integrity was monitored by an Agilent Bioanalyzer 2100 (Agilent technologies, Santa Clara, CA, US). RNeasy micro kit and RNase-Free DNase Set (Cat#74004 and Cat#79254, QIAGEN, GmBH, Germany) were used for the purification of RNA. NimbleGen One-Color DNA Labeling Kit was used for sample labeling with Cy3. To study the anti-inflammatory activity of nitidine chloride, primary mouse BMDC cells were treated with the vehicle only or nitidine chloride for 12 h and then stimulated with the vehicle or LPS 1 μg/ml for another 12 h. NimbleScan v2.5 Software was used for the data extraction and normalization. The fold change analysis between GSM2728729 (control with LPS) and GSM2728730 (nitidine chloride treatment with LPS) resulted in a total of 607 DEGs, including 350 up-regulated and 257 down-regulated genes (**Figure 1**).

Relative signaling pathways and function of nitidine chloride treatment on BMDCs

KEGG pathway and panther pathway annotation: In total, 21 KEGG pathways were identified as significant pathways ($P < 0.05$), wherein the terms of the top five pathways were *mmu04974: protein digestion and absorption, mmu04022: cGMP-PKG signaling pathway, mmu04510: focal adhesion, mmu04010: MAPK signaling pathway and mmu04925: aldosterone synthesis and secretion* (**Table 1**; **Figure 2**). Moreover, panther pathway analysis identified that membrane trafficking regulatory protein (PC00151), metalloprotease (PC00153) and ribosomal protein (PC00202) might be involved in the potential functional pathways of nitidine chloride treatment of BMDCs.

GO biological functional analysis: A total of 142 GO categories, including 72 biological processes (BP), 41 cellular components (CC) and 29

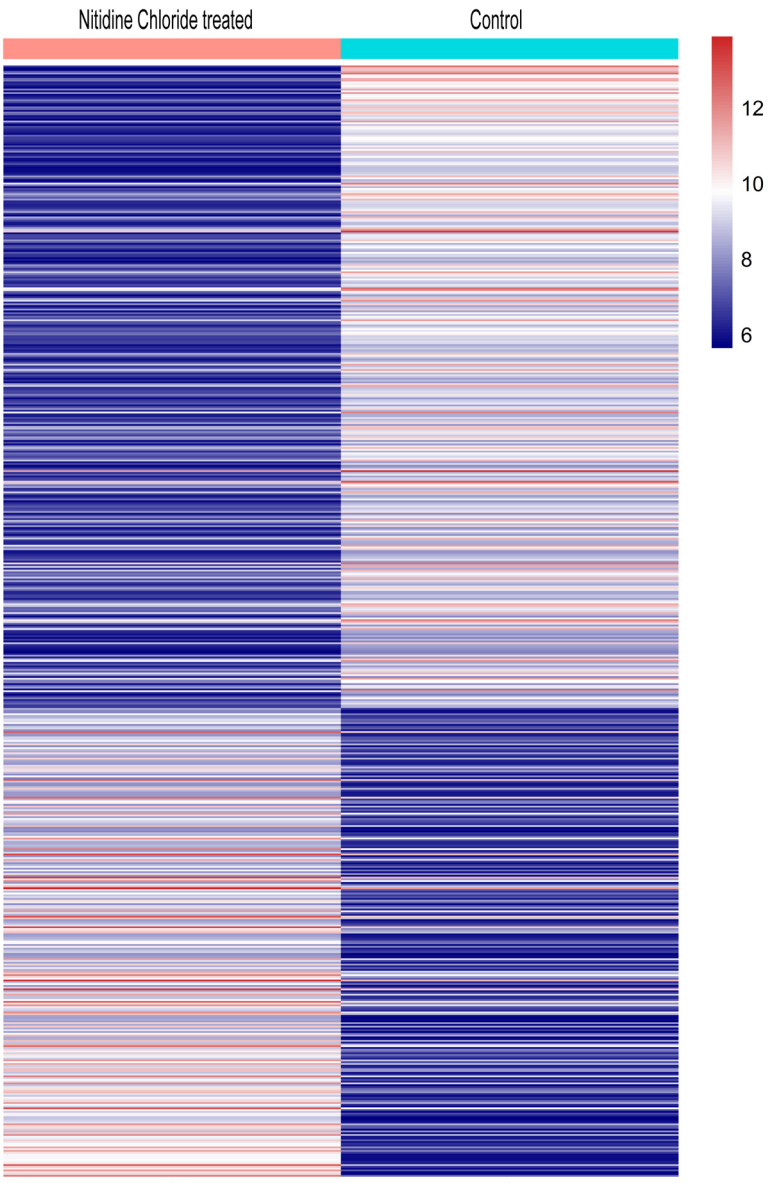

Figure 1. Differentially expressed genes (DEGs) post-nitidine chloride treatment of bone marrow-derived dendritic cells (BMDCs). DEGs were assessed using the NimbleGen Mouse Gene Expression Array (GSE102135) after nitidine chloride treatment of lipopolysaccharide-induced primary mouse BMDCs.

molecular functions (MF), were significantly identified using DAVID ($P < 0.05$). Within the BP category, the term *regulation of Rho protein signal transduction* was most significant ($P = 0.001$). In the CC category, DEGs related to the terms of cytoplasm, synapse, perinuclear region of cytoplasm, membrane and cytoskeleton were highly enriched ($P < 0.001$). In addition, in the MF category, the DEGs were mainly concentrated in the terms *protein binding* and *GTPase activator activity* ($P < 0.001$, **Table 2**; **Figure 3**).

PPI construction: The 607 DEGs were imported into the STRING database, in which 461 proteins were identified. The most significant nodes and edges were included in the PPI network (**Figure 4**). The top 10 protein pairs with high combined scores are shown in **Table 3**.

Identification of correlated CMap compounds

The unknown mechanism of nitidine chloride on LPS-induced BMDCs prompted us to attempt a more systematic approach using the CMap. The aforementioned DEGs were input for CMap analysis, in which 136 chemical drugs were displayed to have the patterns of DEGs expression (permuted *P*-value < 0.05, data not shown) that correlated with those observed after nitidine chloride treatment of LPS-induced BMDCs. The names of the top 20 drugs and their statistics are listed in **Table 4**, where all of the data from single experiments provided by the CMap were combined. Phenoxybenzamine, thioguanosine and resveratrol were the top three drugs (**Table 4**), and the detailed information of these three compounds from different rounds are shown in **Table 5**. Both phenoxybenzamine and thioguanosine were tested four times, and resveratrol was tested nine times (**Tables 4** and **5**). When we ranked the compounds according to only the single test, phenoxybenzamine still remained in the first and second place of the ranking list, followed by 8-azaguanine and irinotecan (**Table 6**; **Figure 5**), with different DEGs being involved (**Table 7**). Those positive enrichment scores represent similar expression patterns of genes induced by chemical drugs from CMap compared with those DEGs in the treatment of LPS-induced BMDCs with nitidine chloride in the current study.

Table 1. The top ten KEGG pathways of the genes influenced by nitidine chloride in bone marrow-derived dendritic cells (BMDCs)

Term	Count	*P* Value	Genes	FDR
mmu04974: Protein digestion and absorption	8	0.002086	SLC8A3, COL9A2, ATP1B2, ATP1A3, CPA3, COL2A1, COL11A2, COL11A1	2.579696
mmu04022: CGMP-PKG signaling pathway	11	0.0026	MEF2C, SLC8A3, EDNRB, ATP1B2, ATP2A3, ATP1A3, PRKCE, IRS1, ITPR1, MYL9, ITPR2	3.205546
mmu04510: Focal adhesion	12	0.003393	DOCK1, VAV3, ITGA6, PGF, ITGAV, COL2A1, ITGA3, COL11A2, COL11A1, MYL9, PRKCB, PARVA	4.163891
mmu04010: MAPK signaling pathway	13	0.00561	MEF2C, IL1R2, DUSP2, NF1, GADD45G, CACNB2, NR4A1, FGF23, MAPK8IP1, FGF1, STK3, PRKCB, MAP2K5	6.797269
mmu04925: Aldosterone synthesis and secretion	7	0.008174	CYP11A1, NR4A1, PRKCE, ITPR1, CAMK1D, PRKCB, ITPR2	9.760639
mmu04020: Calcium signaling pathway	10	0.011431	SLC8A3, EDNRB, ATP2A3, PHKB, SPHK1, ITPKC, ITPR1, PRKCB, ITPR2, HTR2A	13.39984
mmu05412: Arrhythmogenic right ventricular cardiomyopathy (ARVC)	6	0.014839	ITGA6, ITGAV, CACNB2, GJA1, ITGA3, CDH2	17.06174
mmu04972: Pancreatic secretion	7	0.016432	ATP1B2, ATP2A3, ATP1A3, CPA3, ITPR1, PRKCB, ITPR2	18.72507
mmu04514: Cell adhesion molecules (CAMs)	9	0.017898	CLDN7, MPZ, CADM1, ITGA6, CD8A, ITGAV, CDH2, CLDN11, PDCD1	20.22779
mmu04961: Endocrine and other factor-regulated calcium reabsorption	5	0.021366	ATP1B2, ESR1, ATP1A3, DNM1, PRKCB	23.68217

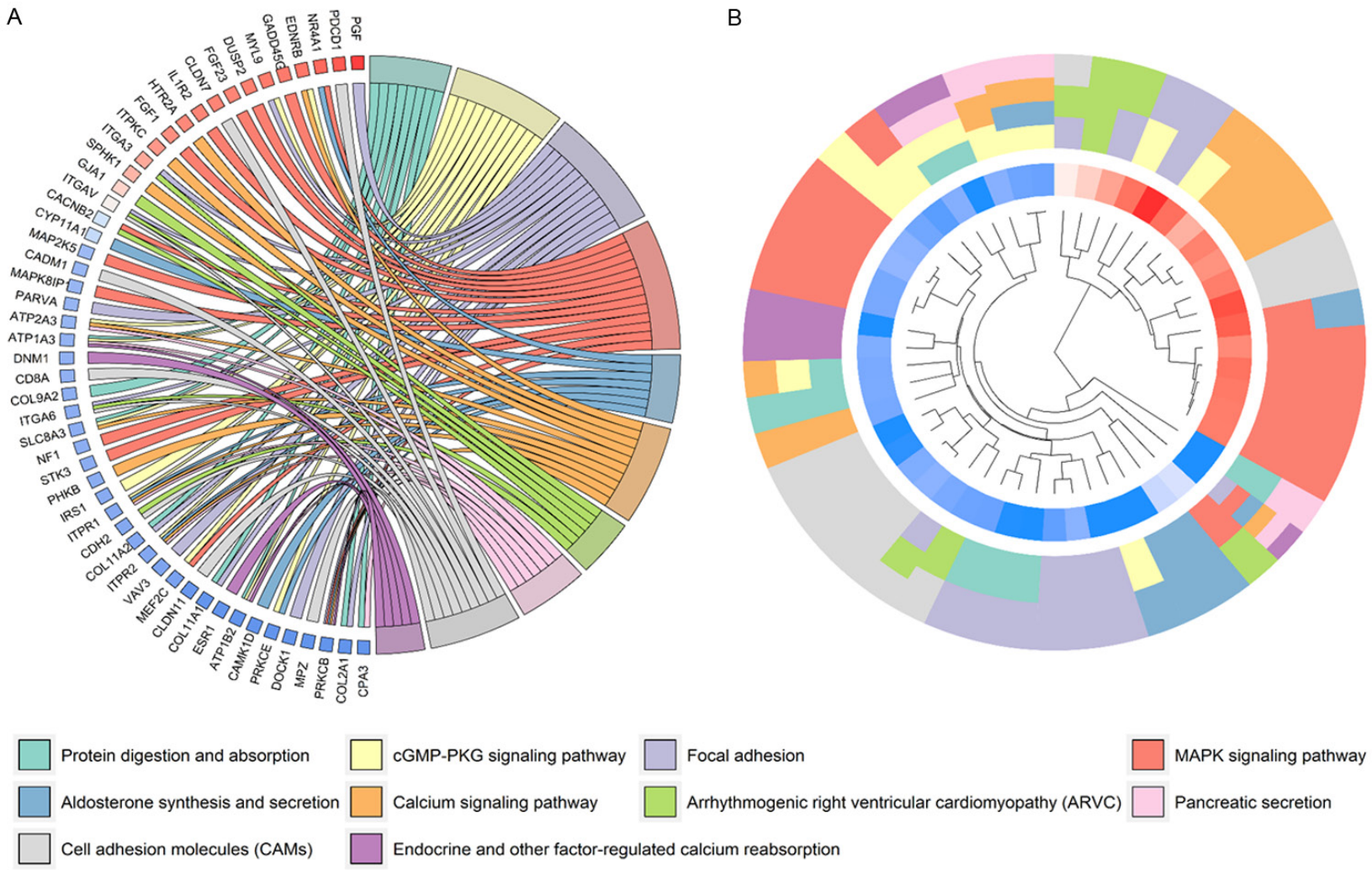

Figure 2. Kyoto Encyclopedia of Genes and Genomes (KEGG) pathway analysis of the genes influenced by nitidine chloride in bone marrow-derived dendritic cells (BMDCs). KEGG pathway analysis was carried out using the DAVID online database to identify the differentially expressed genes after nitidine chloride treatment in lipopolysaccharide-induced primary mouse BMDCs. The GOplot package of R software was used to display the figures.

Table 2. The top eight GO terms of the genes influenced by nitidine chloride in bone marrow-derived dendritic cells (BMDCs)

Category	Term	Count	*P* Value	Genes	FDR
GOTERM_BP_DIRECT	GO: 0035023~regulation of Rho protein signal transduction	8	0.001096	DLC1, PLEKHG4, PLEKHG1, VAV3, ARHGEF6, CDH2, ECT2, FGD4	1.869363
GOTERM_CC_DIRECT	GO: 0005737~cytoplasm	177	8.6E-06	MEF2C, DLC1, SLC8A3, ATP1B2, S100A9, CASK, ITPKC, AURKB, MCM10, CALB2, ANK2, APOD, PPP1R1B, CDCA2, BPNT1, MTUS1, MAP2K5, CDCA3, BCL2L14, C2CD3, GRHL1, IRS1, STK3, FRY, PTHLH, MAPK6, PTRF, CC2D2A, CDCA7L, DST, UNC13B, NRBP2, IL1R2, NEK2, CCDC92, GIPC2, AKAP11, DENND2A, RRAGD, MYT1, KRT24, FUZ, DOCK2, PEG10, CDC42EP1, DOCK1, NDRG4, TCTN2, TRAF4, FGD4, PLAT, VAV3, TRIP4, OSBPL3, WDR7, LPP, FBXO2, SPHK1, NPL, SMYD3, ABHD14A, NR4A1, WRN, TINAGL1, CAMK2N2, 2810417H13RIK, DOCK4, NR1I3, SYNE1, SYNE2, PRICKLE1, NPY, JAZF1, RGS9, AREG, CRYM, EIF4E2, KLF4, TMOD1, CLSPN, KCNAB1, NUAK1, FIGNL1, GJA1, TTLL6, ARHGAP15, SDCBP2, AFMID, MBP, MTHFD1, KIF2C, MSRA, PLEKHB1, SNPH, MGLL, NEURL1A, PRSS36, FGF1, AGAP1, JAKMIP1, CLN3, KIF15, ESR1, ARHGAP24, PRKCE, PIH1D2, ECT2, GAK, PRKCB, ELMO1, ALOX15, EYA2, PTGDS, TNFSF13B, GADD45G, DIS3L2, BUB1B, CAND1, FCRLB, NRGN, RASD1, CTSG, PARVA, CAMK1D, ALOX12, ABLIM2, CPLX1, SLC39A11, FOXM1, CD247, NANOS1, COL2A1, CEP55, CDH2, TRIM10, TPM2, GATSL3, DCT, GPHN, MARVELD2, ALDH1A3, EXOC4, PTN, GPSM2, SH2B2, BCAS3, NEFL, H1F00, SNAP25, TERF1, EX01, WDFY3, WDFY2, CEP192, NF1, ATP1A3, AFF3, KIF18B, BIRC5, RCAN2, ITPR1, GJB2, ITPR2, CCNB1, SCFD1, KCNN1, IRF6, RSRC1, RAB34, DYM, CHN2, MAPK8IP1, CIT, PES1, DNM1, KIF20A, HTR2A	0.011968
GOTERM_CC_DIRECT	GO: 0045202~synapse	27	1.51E-05	CLCN3, CPLX1, CADM1, CASK, CDH2, CALB2, SLC1A2, GPHN, SH2D5, ANK2, SNPH, EXOC4, MGLL, LGI3, NEURL1A, SNAP25, PLAT, DLGAP1, ATP1A3, DENND1A, ITGA3, SEMA4F, CHN2, MAPK8IP1, NRGN, UNC13B, DNM1	0.021002
GOTERM_CC_DIRECT	GO: 0048471~perinuclear region of cytoplasm	32	3.52E-05	SLC8A3, PAM, OLFM4, NANOS1, ANGEL1, LNPEP, APOD, ANK2, PTN, NEURL1A, SNAP25, TRAF4, MT3, ESR1, ITGA3, PRKCE, 2810417H13RIK, ITPR1, VTI1A, GAK, EPHA5, SYNE1, TNFSF13B, NPY, PTGDS, CX3CR1, RAB34, CCR2, BUB1B, MAPK8IP1, RASD1, DST	0.048999
GOTERM_CC_DIRECT	GO: 0016020~membrane	181	4.75E-05	DLC1, SLC8A3, MPZL2, CADM1, PGF, ATP1B2, SLC22A15, S100A9, CASK, ILDR1, CSPG5, ANK2, SH2D5, ST3GAL6, PELI2, RAB26, GNG4, MTUS1, PHRF1, OSBP2, ATRNL1, NBAS, SLCO4A1, SCUBE1, VTI1A, CRHR1, PTRF, CD33, CCR3, CX3CR1, CCR2, PTGFRN, DST, CD300LB, UNC13B, IL1R2, PAM, CLCN3, IFITM1, CYP2B9, LY6G6C, TMEM82, CACNB2, FXYD6, DOCK2, CDC42EP1, DOCK1, ITGAV, ADAM33, HNRNPC, TCTN2, HIST1H4I, TRAF4, OSBPL3, FBXO2, SPHK1, NUF2, TNFRSF13C, DENND1A, ABHD14A, ITGA3, EN2, DOCK4, EPHA5, SYNE1, SYNE2, PRICKLE1, ITGA6, ATP2A3, FREM2, G0LGA7B, TM4SF20, RGS9, AREG, CEND1, KLRB1B, TMOD1, CLDN7, MCHR1, CD8A, KCNAB1, PHKB, SUSD2, PIP5K1B, GJA1, ARHGAP15, LSR, DDR2, LGR5, GPR89, PDCD1, MBP, TMEM177, MTHFD1, LNPEP, EDNRB, KIF2C, SLC1A2, MSRA, PLEKHB1, TMEM108, TMEM171, SLC24A3, SNPH, MGLL, RHOD, NEURL1A, LBP, AGAP1, IRGC1, SLC43A2, JAKMIP1, CLN3, CYP11A1, KIF15, ESR1, SLC24A5, PRKCE, NDUFA11, GAK, PRKCB, ELMO1, CLEC16A, ZDHHC14, ALOX15, PTGDS, TNFSF13B, TLCD1, SEMA4F, SBF2, PLXDC2, ADAM18, CAND1, RASD1, CTSG, DEGS2, PARVA, ALOX12, GPR183, SLC39A11, CD247, CEP55, CLDN11, CDH2, CDKAL1, GPRC5A, GPR4, TPCN1, DCT, ZDHHC23, GPHN, LECT1, MARVELD2, TBC1D5, EXOC4, PTN, SH2B2, POPDC3, 4932438A13RIK, RNF122, SNAP25, WDFY3, DLGAP1, MPZ, NF1, ATP1A3, ITPR1, GJB2, ITPR2, CCNB1, PROM1, SCFD1, KCNN1, CDON, RAB34, DYM, CHN2, MAPK8IP1, CIT, PES1, HTR2A	0.066121
GOTERM_CC_DIRECT	GO: 0005856~cytoskeleton	41	0.000337	NEK2, CCDC92, S100A9, TTLL6, CEP55, AURKB, DENND2A, TPM2, FUZ, KIF2C, GPHN, DOCK2, CDC42EP1, ANK2, GPSM2, TCTN2, BCAS3, TRAF4, JAKMIP1, TERF1, FGD4, TRIP4, C2CD3, KIF15, KIF18B, BIRC5, ARHGAP24, PRKCE, ECT2, FRY, CCNB1, NR1I3, SYNE1, SYNE2, KRT16, CC2D2A, DST, DNM1, KIF20A, PARVA, TMOD1	0.467394
GOTERM_MF_DIRECT	GO: 0005515~protein binding	117	0.000243	MEF2C, CADM1, THRB, CASK, RORB, AURKB, ANK2, SH2D5, KIFAP3, LGI3, PELI2, RAB26, MAP2K5, COCH, C2CD3, ATRNL1, FGF23, IRS1, MAPK6, KRT16, CCR3, CC2D2A, CCR2, DST, CD300LB, CHGB, OLFM4, NEK2, CACNB2, MYT1, DOCK1, CDC42EP1, SERPINA1B, NDRG4, RHOBTB1, TCTN2, VAV3, CPNE4, LPP, MAFB, FBXO2, SMYD3, DENND1A, NR4A1, DOCK7, ITGA3, WRN, EPHA5, SYNE1, NR1I3, PRICKLE1, ITGA6, ATP2A3, FREM2, EBF1, RGS9, KLRB1B, CEND1, KLF4, CLDN7, KCNAB1, UVRAG, PIP5K1B, GJA1, TTLL6, KRT33A, PDCD1, LNPEP, EDNRB, PLEKHB1, SAA1, NEURL1A, FGF1, CLN3, ESR1, PRKCE, ECT2, GAK, PRKCB, ELMO1, SEMA4F, GADD45G, BUB1B, CAND1, PARVA, FKBP7, FOXM1, CD247, CEP55, CLDN11, CDH2, TRIM10, TPM2, GPRC5A, GPHN, ACAN, EXOC4, GPSM2, SH2B2, SNAP25, NEFL, TERF1, WDFY2, NF1, BIRC5, ITPR1, GJB2, ITPR2, CCNB1, IQCF1, RSRC1, CDON, RAB34, MAPK8IP1, CIT, PES1, DNM1	0.358697
GOTERM_MF_DIRECT	GO: 0005096~GTPase activator activity	15	0.000496	DLC1, NF1, ARHGAP19, ARHGAP24, ARHGAP15, ECT2, TBC1D22A, DOCK4, DOCK2, DOCK1, CDC42EP1, TBC1D5, CHN2, RGS9, AGAP1	0.731331

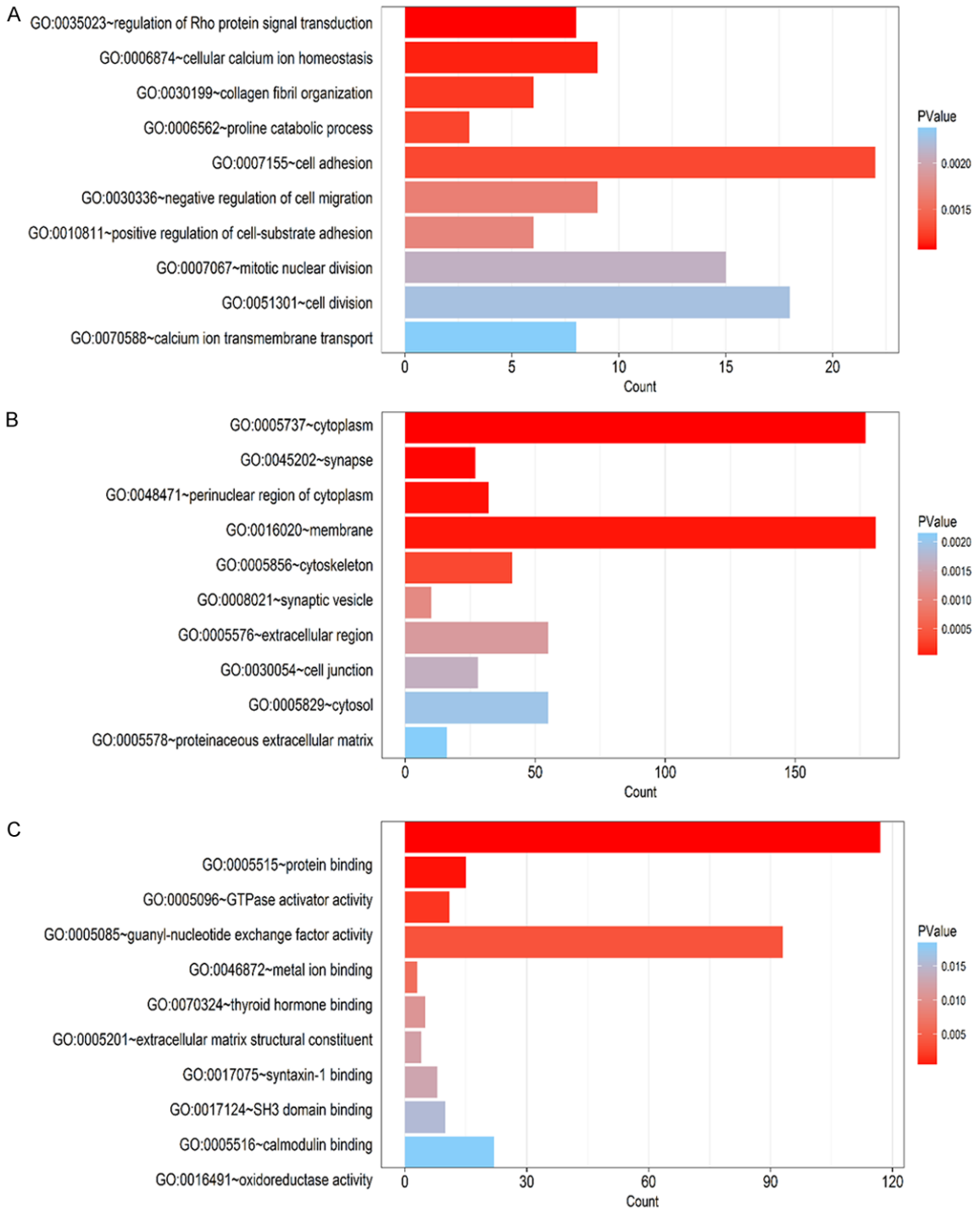

Figure 3. Gene ontology (GO) enrichment analysis of the genes influenced by nitidine chloride in bone marrow-derived dendritic cells (BMDCs). GO analysis was carried out using the DAVID online database to display the differentially expressed genes after nitidine chloride treatment on lipopolysaccharide-induced primary mouse BMDCs. The ggplot2 package of R software was used to display the figures.

Discussion

In the current study, we identified the DEGs observed post-nitidine chloride treatment on LPS-stimulated BMDCs and found that several pathways related to inflammation could play pivotal roles in the effect of nitidine chloride. Furthermore, by connective mapping with CM-

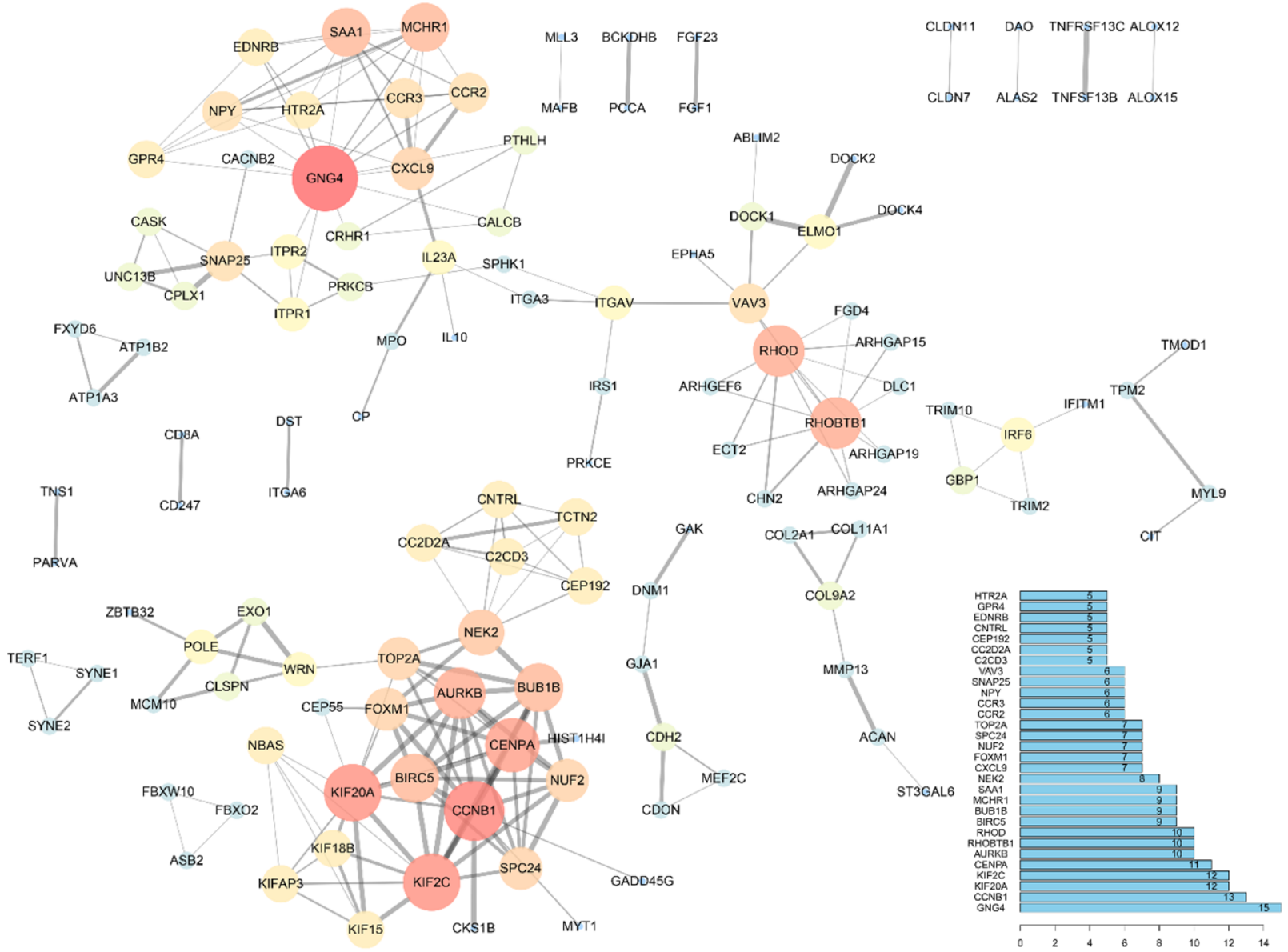

Figure 4. Protein-protein interaction (PPI) network of the genes influenced by nitidine chloride in bone marrow-derived dendritic cells (BMDCs). PPI analysis was carried out using the STRING online database to display the PPI network of the differentially expressed genes after nitidine chloride treatment in lipopolysaccharide-induced primary mouse BMDCs. The Cytoscape and ggplot2 packages of R were used to visualize the results of PPI.

Table 3. The strongest 10 PPI nodes identified using STRING in the genes influenced by nitidine chloride treatment of bone marrow-derived dendritic cells (BMDCs)

Node 1	Node 2	Coexpression	Experimentally determined interaction	Database-annotated	Automated text mining	Combined score
Birc5	Aurkb	0.847	0.421	0.95	0.901	0.999
Bub1b	Aurkb	0.897	0.912	0.9	0.824	0.999
Cenpa	Aurkb	0.657	0.401	0.95	0.873	0.998
Kif2c	Aurkb	0.714	0.115	0.95	0.859	0.998
Dock1	Elmo1	0.05	0.795	0.941	0.901	0.998
Ccnb1	Aurkb	0.911	0.17	0.9	0.651	0.997
Spc24	Nuf2	0.554	0.554	0.9	0.897	0.997
Tnfrsf13c	Tnfsf13b	0.134	0.776	0.9	0.889	0.997
Dock2	Elmo1	0.053	0.795	0.883	0.897	0.997
Ccnb1	Bub1b	0.856	0.1	0.95	0.5	0.996

Table 4. Top 20 CMap compounds matching the DEGs identified post-nitidine chloride treatment of BMDCs

Rank	CMap name	Mean	N	Enrichment	*P* value	Specificity	Percent non-null
1	Phenoxybenzamine	0.956	4	0.998	0	0	100
2	Thioguanosine	0.747	4	0.946	0	0.0059	100
3	Resveratrol	0.675	9	0.81	0	0.0245	100
4	Trichostatin A	0.21	182	0.252	0	0.801	59
5	PHA-00745360	-0.363	8	-0.775	0.00002	0	100
6	Irinotecan	0.882	3	0.982	0.00004	0.0818	100
7	Prochlorperazine	0.443	16	0.557	0.00006	0.0728	81
8	Thioridazine	0.416	20	0.521	0.00006	0.2101	75
9	Thiostrepton	0.636	4	0.893	0.00012	0.0294	100
10	Ciclopirox	0.61	4	0.888	0.00016	0.029	100
11	Luteolin	0.701	4	0.886	0.00016	0.0146	100
12	Trifluoperazine	0.472	16	0.495	0.0003	0.2115	81
13	Prestwick-692	-0.54	4	-0.875	0.00054	0.0068	100
14	8-azaguanine	0.704	4	0.858	0.00054	0.0473	100
15	Sulconazole	0.647	4	0.854	0.00064	0.0063	100
16	Adiphenine	-0.502	5	-0.798	0.0007	0.0887	100
17	Apigenin	0.639	4	0.852	0.00072	0.0391	100
18	Guanabenz	-0.486	5	-0.791	0.00078	0.0154	100
19	Etoposide	0.697	4	0.846	0.0008	0.0615	100
20	Daunorubicin	0.598	4	0.834	0.00115	0.0657	100

Note: N, number of cell lines in the CMap database. The mean was calculated from all available CMap data for a single drug.

ap analysis, several known compounds that had similar molecular mechanisms to that of nitidine chloride were found, including phenoxybenzamine, thioguanosine, resveratrol, 8-azaguanine and irinotecan. These findings could assist in the identification of a novel potential mechanism for the treatment of inflammatory diseases with nitidine chloride.

The anti-inflammatory effects of seven benzophenanthridine alkaloids from Zanthoxylum nitidum (Roxb.) DC have been confirmed previously as being similar to that of hydrocortisone, including the pentacyclic alkaloid nitidine chloride [21]. Nitidine chloride also achieves anti-inflammatory activity by suppressing TNF-α, IL-1β, and IL-6 production related to down-regulated NF-κB and MAPK signaling pathways in RAW 264.7 murine macrophages. Nitidine chloride has additionally been found to suppress LPS-induced TNF alpha, IL-1beta and IL-6 production through inhibition of the phosphoryla-

Table 5. Detailed information on the top 3 CMap compounds matching the DEGs identified post-nitidine chloride treatment of BMDCs

Rank	Batch	CMap name	Dose	Cell	Score	Up	Down	Instance ID
1	758	Phenoxybenzamine	12 μM	MCF7	1	0.172	-0.277	5613
2	726	Phenoxybenzamine	12 μM	MCF7	0.997	0.198	-0.25	5248
6	755	Phenoxybenzamine	12 μM	MCF7	0.955	0.148	-0.28	6451
16	713	Phenoxybenzamine	12 μM	PC3	0.871	0.164	-0.227	4652
13	630	Thioguanosine	13 μM	HL60	0.878	0.217	-0.177	1264
57	653	Thioguanosine	13 μM	MCF7	0.791	0.159	-0.196	2619
234	707	Thioguanosine	13 μM	MCF7	0.675	0.152	-0.15	4989
333	710	Thioguanosine	13 μM	PC3	0.643	0.149	-0.14	6643
18	502	Resveratrol	10 μM	MCF7	0.862	0.196	-0.19	958
22	657	Resveratrol	18 μM	MCF7	0.848	0.192	-0.189	2865
58	640	Resveratrol	18 μM	HL60	0.79	0.157	-0.197	1715
86	107	Resveratrol	50 μM	MCF7	0.769	0.194	-0.151	622
186	504	Resveratrol	10 μM	MCF7	0.699	0.12	-0.194	841
479	738	Resveratrol	18 μM	MCF7	0.601	0.143	-0.127	5509
964	95	Resveratrol	50 μM	MCF7	0.517	0.105	-0.127	595
1106	719	Resveratrol	18 μM	PC3	0.498	0.079	-0.144	5084
1167	90	Resveratrol	50 μM	PC3	0.489	0.077	-0.143	662

Table 6. Top 20 CMap compounds matching the DEGs identified post-nitidine chloride treatment of BMDCs

Rank	Batch	CMap name	Dose	Cell	Score	Up	Down	Instance ID
1	758	Phenoxybenzamine	12 μM	MCF7	1	0.172	-0.277	5613
2	726	Phenoxybenzamine	12 μM	MCF7	0.997	0.198	-0.25	5248
3	629	8-azaguanine	26 μM	HL60	0.996	0.273	-0.174	1833
4	1082	Irinotecan	100 μM	MCF7	0.967	0.207	-0.227	7498
5	664	Sanguinarine	12 μM	HL60	0.964	0.261	-0.172	2927
6	755	Phenoxybenzamine	12 μM	MCF7	0.955	0.148	-0.28	6451
7	1090	Irinotecan	100 μM	MCF7	0.931	0.142	-0.276	7530
8	644	Picrotoxinin	14 μM	HL60	0.912	0.262	-0.147	2161
9	664	Fursultiamine	9 μM	HL60	0.91	0.241	-0.167	2929
10	665	Pivampicillin	9 μM	HL60	0.9	0.257	-0.147	2945
11	649	Meclofenoxate	14 μM	HL60	0.9	0.246	-0.158	2546
12	505	5109870	25 μM	MCF7	0.879	0.208	-0.186	904
13	630	Thioguanosine	13 μM	HL60	0.878	0.217	-0.177	1264
14	622	Labetalol	11 μM	HL60	0.873	0.24	-0.152	1550
15	665	Pyrvinium	3 μM	HL60	0.872	0.236	-0.155	2957
16	713	Phenoxybenzamine	12 μM	PC3	0.871	0.164	-0.227	4652
17	665	Iopanoic acid	7 μM	HL60	0.865	0.24	-0.148	2965
18	502	Resveratrol	10 μM	MCF7	0.862	0.196	-0.19	958
19	660	Nitrendipine	11 μM	HL60	0.858	0.243	-0.142	3087
20	660	(-)-atenolol	15 μM	HL60	0.858	0.244	-0.141	3067

Note: N, number of cell lines in the CMap database. The score was calculated from an individual CMap test for a single drug.

tion of MAPK and the translocation of p65 [44]. Furthermore, in mouse-derived bone marrow monocytes (BMMs), nitidine chloride inhibited RANKL-prompted multinucleated tartrate-resistant acid phosphatase (TRAP)-positive osteoclast construction and bone resorption depen-

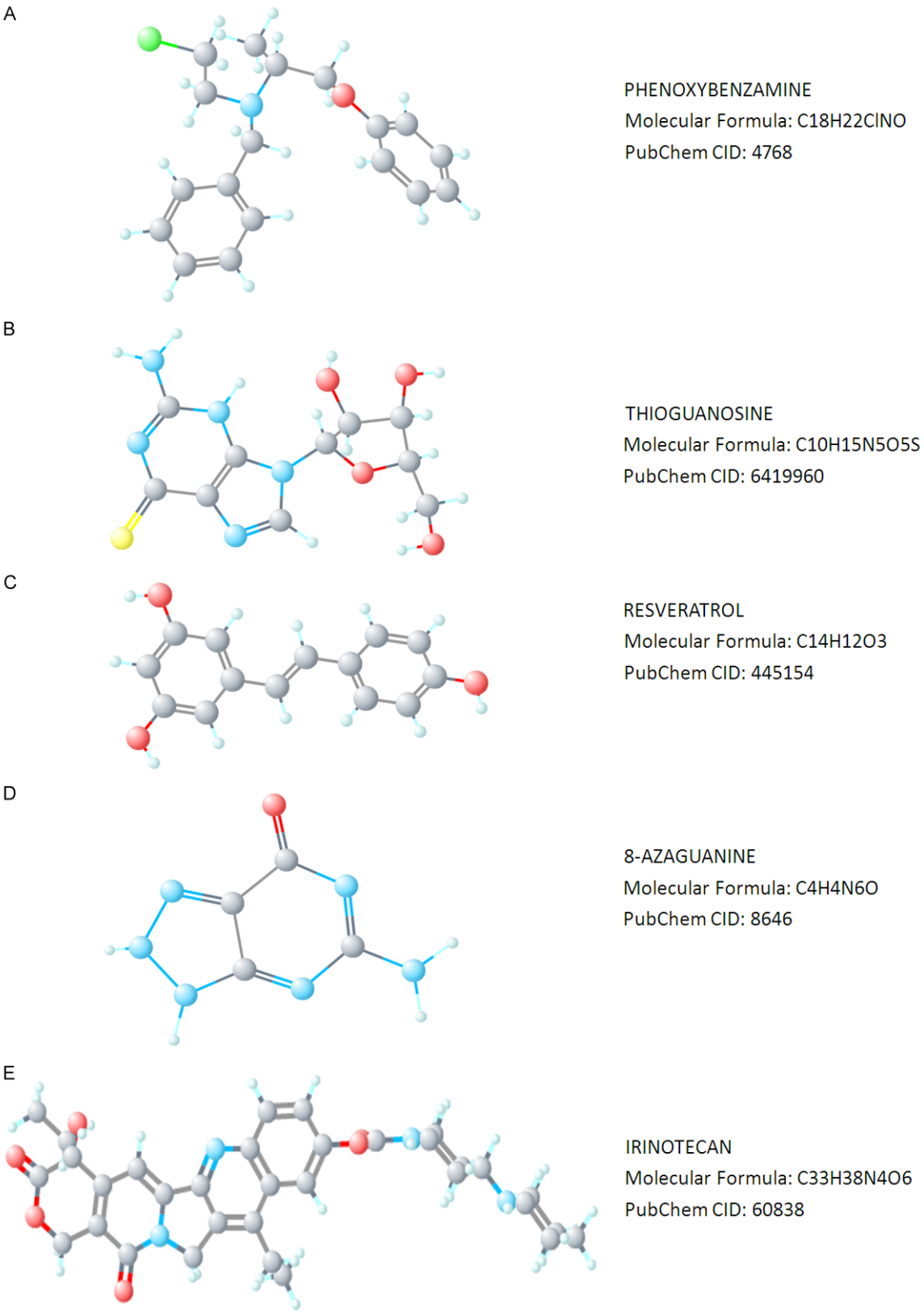

Figure 5. The 3D conformers of the five compounds similar to nitidine chloride in bone marrow-derived dendritic cells (BMDCs). The 3D structures of the five compounds were provided by PubChem (https://pubchem.ncbi.nlm.nih.gov/compound). A: PHENOXYBENZAMINE; B: THIOGUANOSINE; C: RESVERATROL; D: 8-AZAGUANINE; E: IRINOTECAN.

Table 7. Genes related to the Top 3 CMap compounds from **Table 6**

Phenoxybenzamine		8-azaguanine		Irinotecan	
Up	Down	Up	Down	Up	Down
GEM	ATAD5	INHBA	NCAPH	LIF	NRP1
POPDC3	CTNND2	CREM	TTF2	DDIT4	ATAD2
DDIT4	MXD3	IL1B	OIP5	GP6	NDC80
HBEGF	MBD5	GEM	GPSM2	HOXA5	DTL
CREM	NCAPH	DUSP4	CCNB1	IRF7	NCAPH
EN2	WDR7	CXCL2	DLGAP5	IP6K2	CENPI
IP6K2	FBXO5	TIMP1	KIF15	EN2	BRIP1
TRIB3	GPHN	TRIB3	MNS1	TEX14	BUB1B
DLC1	EGR3	HBEGF	GFI1	DUSP14	LARGE
STK3	CENPI	NR4A1	CDC7	VASH1	NCAPG

dent on the dosage of nitidine chloride. Nitidine chloride decreased the level of osteoclast marker genes, such as cathepsin K, D2, calcitonin receptor, NFATc1, and TRAP. Additionally, NC suppressed RANKL-activated NF-κB and NFATc1 signaling pathways, which could also be involv-ed in the progress of inflammation [45]. Nitidine chloride repressed VEGF-induced endothelial cell proliferation, migration, and tubular structure formation in vitro in a dose-dependent manner and intensely decreased VEGF triggered neovascularization in mouse cornea and Matrigel plugs in vivo. This angiogenesis suppression mediated by nitidine chloride was well understood by the inhibition of Janus kinase 2/STAT3 signaling and the STAT3 DNA-binding capacity in endothelial cells. Additionally, nitidine chloride inhibited the constituently activated STAT3 protein, its DNA-binding activity, and the expression of STAT3-dependent target genes-for instance, cyclin D1, Bcl-xL, and VEGF in malignancies [46]-which could also be mirrored in the mediation procedure of some types of inflammation. Nevertheless, the anti-inflammatory mechanism of nitidine chloride has still not been completely interpreted. In the current study, we found that the DEGs identified post-nitidine chloride treatment of LPS-stimulated BMDCs were enriched in several well-known pathways determined by KEGG analysis-for instance, *protein digestion and absorption*, the cGMP-PKG signaling pathway, focal adhesion, the MAPK signaling pathway and aldosterone synthesis and secretion, which have been established to play essential parts in the inflammatory process [47-52]. The anti-inflammatory function of nitidine chloride could be determined via targeting these pathways; however, more in-depth validations are still required.

In addition to the potential signaling pathways of nitidine chloride, we also examined whether NC performs its function consistent with the characteristics of any other well-known compound using the Connectivity Map tool. The gene signature identified post-nitidine chloride treatment served as an unordered query which was input into a customized database including differential gene-expression experiments with responses to a wide range of over 1,300 small molecules across of spectrum of concentrations, durations, and cell lines. A score for each experiment that measured "closeness" between the signature and the experiment was provided. Thus, by comparing the microarray data from over 1,309 small molecules provided by CMap to our selected 607 DEGs, a list of compounds ranked from highly positively correlated (similar gene expression pattern to that of the phenotype of interest) to strongly negatively correlated was obtained. Positively correlated genes had similar gene patterns to those of modulation by nitidine chloride in BMDCs. In the current study, it is interesting to note that five novel compounds (phenoxybenzamine, thioguanosine, resveratrol, 8-azaguanine and irinotecan) were determined as holding the biggest potential to be involved in the complex biological process of nitidine chloride treatment. Among these five compounds, four were previously well-known to have anti-inflammation properties, including phenoxybenzamine [53-55], thioguanosine [56, 57], resveratrol [58-62] and irinotecan [63, 64]. However, the ability of 8-azaguanine to treat inflammation has rarely been reported. Some types of mycobacterium tuberculosis were known to be potentially inhibited by 8-azaguanine [65]. Therefore, nitidine chloride could play a similar anti-inflammatory role compared to those of the aforementioned compounds, but it may also vary in its mechanism.

In summary, different genes have been implicated in the nitidine chloride-mediated immunomodulatory function in the anti-inflammation procedure targeting several key pathways related to inflammation. The anti-inflammation properties of nitidine chloride could be mirrored by

some known drugs, which could help to identify the underlying mechanism of nitidine chloride treatment.

Acknowledgements

This study was partly supported by the funds of National Natural Science Foundation of China (NSFC 81860717), Natural Science Foundation of Guangxi, China (2018GXNSFAA294025), Guangxi First-class Discipline Project for Pharmaceutical Sciences (No. GXFCDP-PS-2018), Medical Excellence Award Funded by the Creative Research Development Grant from the First Affiliated Hospital of Guangxi Medical University, Guangxi Degree and Postgraduate Education Reform and Development Research Projects, China (JGY2019050) and Guangxi Zhuang Autonomous Region Health and Family Planning Commission Self-financed Scientific Research Project (Z20180979).

Disclosure of conflict of interest

None.

Address correspondence to: Gang Chen, Department of Pathology, The First Affiliated Hospital of Guangxi Medical University, Shuangyong Road 6, Nanning 530021, Guangxi Zhuang Autonomous Region, P. R. China. Tel: +86-771-5356534; Fax: +86-771-5356534; E-mail: chengang@gxmu.edu.cn

References

[1] Yao Y, Wu J, Gu T, Cheng Y and Li G. Comparative analysis of the interaction of HSPs in dendritic cells, macrophages, RGM-1 cells infected by helicobacter pylori. Am J Transl Res 2016; 8: 4184-4194.

[2] Shi Q, Yin Z, Liu P, Zhao B, Zhang Z, Mao S, Wei T, Rao M, Zhang L and Wang S. Cilostazol suppresses IL-23 production in human dendritic cells via an AMPK-dependent pathway. Cell Physiol Biochem 2016; 40: 499-508.

[3] Garcia EP, Tiscornia I, Libisch G, Trajtenberg F, Bollati-Fogolin M, Rodriguez E, Noya V, Chiale C, Brossard N, Robello C, Santinaque F, Folle G, Osinaga E and Freire T. MUC5B silencing reduces chemo-resistance of MCF-7 breast tumor cells and impairs maturation of dendritic cells. Int J Oncol 2016; 48: 2113-2123.

[4] Xu X, Gao X, Zhao X, Liao Y, Ji W, Li Q and Li J. PU.1-silenced dendritic cells induce mixed chimerism and alleviate intestinal transplant rejection in rats via a Th1 to Th2 shift. Cell Physiol Biochem 2016; 38: 220-228.

[5] Yan J, Schmid E, Hosseinzadeh Z, Honisch S, Shumilina E, Fuchs J and Lang F. Impact of janus kinase 3 on cellular ca release, store operated Ca(2+) entry and Na(+)/Ca(2+) exchanger activity in dendritic cells. Cell Physiol Biochem 2015; 36: 2287-2298.

[6] Wang H, Hu W, Liang Z, Zeng L, Li J, Yan H, Yang P, Liu Z and Wang L. Thiol peroxiredoxin, a novel allergen from Bombyx mori, modulates functions of macrophages and dendritic cells. Am J Transl Res 2016; 8: 5320-5329.

[7] Mikyskova R, Stepanek I, Indrova M, Bieblova J, Simova J, Truxova I, Moserova I, Fucikova J, Bartunkova J, Spisek R and Reinis M. Dendritic cells pulsed with tumor cells killed by high hydrostatic pressure induce strong immune responses and display therapeutic effects both in murine TC-1 and TRAMP-C2 tumors when combined with docetaxel chemotherapy. Int J Oncol 2016; 48: 953-964.

[8] Zhou Y, Pasham V, Chatterjee S, Rotte A, Yang W, Bhandaru M, Singh Y and Lang F. Regulation of Na(+)/H(+) exchanger in dendritic cells by Akt1. Cell Physiol Biochem 2015; 36: 1237-1249.

[9] Guo M, Yan R, Wang C, Shi H, Sun M, Guo S and Xiao C. IFN regulatory factor-1 modulates the function of dendritic cells in patients with acute coronary syndrome. Cell Physiol Biochem 2015; 36: 599-610.

[10] Zheng Y, Cai W, Zhou S, Xu L and Jiang C. Protective effect of bone marrow derived mesenchymal stem cells in lipopolysaccharide-induced acute lung injury mediated by claudin-4 in a rat model. Am J Transl Res 2016; 8: 3769-3779.

[11] Yan JK, Zhu J, Gu BL, Yan WH, Xiao YT, Zhou KJ, Wen J, Wang Y and Cai W. Soybean oil-based lipid emulsion increases intestinal permeability of lipopolysaccharide in caco-2 cells by downregulation of p-glycoprotein via ERK-FOXO 3a pathway. Cell Physiol Biochem 2016; 39: 1581-1594.

[12] Cao Z, Yao Q and Zhang S. MiR-146a activates WAVE2 expression and enhances phagocytosis in lipopolysaccharide-stimulated RAW264.7 macrophages. Am J Transl Res 2015; 7: 1467-1474.

[13] Han C, Ding Z, Shi H, Qian W, Hou X and Lin R. The role of probiotics in lipopolysaccharide-induced autophagy in intestinal epithelial cells. Cell Physiol Biochem 2016; 38: 2464-2478.

[14] Yin N, Peng Z, Li B, Xia J, Wang Z, Yuan J, Fang L and Lu X. Isoflurane attenuates lipopolysaccharide-induced acute lung injury by inhibiting ROS-mediated NLRP3 inflammasome activation. Am J Transl Res 2016; 8: 2033-2046.

[15] Li S, Guo L, Qian P, Zhao Y, Liu A, Ji F, Chen L, Wu X and Qian G. Lipopolysaccharide induces

autophagic cell death through the PERK-dependent branch of the unfolded protein response in human alveolar epithelial A549 cells. Cell Physiol Biochem 2015; 36: 2403-2417.
[16] Kim JS and Jobin C. The flavonoid luteolin prevents lipopolysaccharide-induced NF-kappaB signalling and gene expression by blocking IkappaB kinase activity in intestinal epithelial cells and bone-marrow derived dendritic cells. Immunology 2005; 115: 375-387.
[17] Dat le D, Thao NP, Tai BH, Luyen BT, Kim S, Koo JE, Koh YS, Cuong NT, Thanh NV, Cuong NX, Nam NH, Kiem PV, Minh CV and Kim YH. Chemical constituents from Kandelia candel with their inhibitory effects on pro-inflammatory cytokines production in LPS-stimulated bone marrow-derived dendritic cells (BMDCs). Bioorg Med Chem Lett 2015; 25: 1412-1416.
[18] Wong TH, Chen HA, Gau RJ, Yen JH and Suen JL. Heme oxygenase-1-expressing dendritic cells promote foxp3+ regulatory T cell differentiation and induce less severe airway inflammation in murine models. PLoS One 2016; 11: e0168919.
[19] Dong Y, Arif A, Olsson M, Cali V, Hardman B, Dosanjh M, Lauer M, Midura RJ, Hascall VC, Brown KL and Johnson P. Endotoxin free hyaluronan and hyaluronan fragments do not stimulate TNF-alpha, interleukin-12 or upregulate co-stimulatory molecules in dendritic cells or macrophages. Sci Rep 2016; 6: 36928.
[20] Zhang W, Yu X, Kwak M, Xu L, Zhang L, Yu Q and Jin JO. Maturation of dendritic cells by pullulan promotes anti-cancer effect. Oncotarget 2016; 7: 44644-44659.
[21] Hu J, Zhang WD, Liu RH, Zhang C, Shen YH, Li HL, Liang MJ and Xu XK. Benzophenanthridine alkaloids from zanthoxylum nitidum (Roxb.) DC, and their analgesic and anti-inflammatory activities. Chem Biodivers 2006; 3: 990-995.
[22] Wang CF, Fan L, Tian M, Du SS, Deng ZW, Feng JB, Wang YY and Su X. Cytotoxicity of benzophenanthridine alkaloids from the roots of zanthoxylum nitidum (Roxb.) DC. var. fastuosum how ex huang. Nat Prod Res 2015; 29: 1380-1383.
[23] Beck A, Eberherr C, Hagemann M, Cairo S, Haberle B, Vokuhl C, von Schweinitz D and Kappler R. Connectivity map identifies HDAC inhibition as a treatment option of high-risk hepatoblastoma. Cancer Biol Ther 2016; 17: 1168-1176.
[24] Yu J, Putcha P and Silva JM. Recovering drug-induced apoptosis subnetwork from connectivity map data. Biomed Res Int 2015; 2015: 708563.
[25] Huang H, Nguyen T, Ibrahim S, Shantharam S, Yue Z and Chen JY. DMAP: a connectivity map database to enable identification of novel drug repositioning candidates. BMC Bioinformatics 2015; 16 Suppl 13: S4.
[26] Brum AM, van de Peppel J, van der Leije CS, Schreuders-Koedam M, Eijken M, van der Eerden BC and van Leeuwen JP. Connectivity map-based discovery of parbendazole reveals targetable human osteogenic pathway. Proc Natl Acad Sci U S A 2015; 112: 12711-12716.
[27] Wang K, Weng Z, Sun L, Sun J, Zhou SF and He L. Systematic drug safety evaluation based on public genomic expression (connectivity map) data: myocardial and infectious adverse reactions as application cases. Biochem Biophys Res Commun 2015; 457: 249-255.
[28] Huang Y, Tao Y, Li X, Chang S, Jiang B, Li F and Wang ZM. Bioinformatics analysis of key genes and latent pathway interactions based on the anaplastic thyroid carcinoma gene expression profile. Oncol Lett 2017; 13: 167-176.
[29] Cao B, Feng L, Lu D, Liu Y, Liu Y, Guo S, Han N, Liu X, Mao Y, He J, Cheng S, Gao Y and Zhang K. Prognostic value of molecular events from negative surgical margin of non-small-cell lung cancer. Oncotarget 2017; 8: 53642-53653.
[30] Fan Q and Liu B. Identification of a RNA-Seq based 8-long non-coding RNA signature predicting survival in esophageal cancer. Med Sci Monit 2016; 22: 5163-5172.
[31] Wang P, Cui J, Wen J, Guo Y, Zhang L and Chen X. Cisplatin induces hepG2 cell cycle arrest through targeting specific long noncoding RNAs and the p53 signaling pathway. Oncol Lett 2016; 12: 4605-4612.
[32] Safari-Alighiarloo N, Rezaei-Tavirani M, Taghizadeh M, Tabatabaei SM and Namaki S. Network-based analysis of differentially expressed genes in cerebrospinal fluid (CSF) and blood reveals new candidate genes for multiple sclerosis. Peer J 2016; 4: e2775.
[33] Mi H, Huang X, Muruganujan A, Tang H, Mills C, Kang D and Thomas PD. PANTHER version 11: expanded annotation data from gene ontology and reactome pathways, and data analysis tool enhancements. Nucleic Acids Res 2017; 45: D183-D189.
[34] Makoukji J, Makhoul NJ, Khalil M, El-Sitt S, Aldin ES, Jabbour M, Boulos F, Gadaleta E, Sangaralingam A, Chelala C, Boustany RM and Tfayli A. Gene expression profiling of breast cancer in lebanese women. Sci Rep 2016; 6: 36639.
[35] Han D, Chen Y, Kou Y, Weng J, Chen B, Yu Y, Zhang P and Jiang B. Profiling of the dynamically altered gene expression in peripheral nerve injury using NGS RNA sequencing technique. Am J Transl Res 2016; 8: 871-884.
[36] Liu Y, Ni R, Zhang H, Miao L, Wang J, Jia W and Wang Y. Identification of feature genes for

smoking-related lung adenocarcinoma based on gene expression profile data. Onco Targets Ther 2016; 9: 7397-7407.
[37] Li M and Wu L. Functional analysis of keratinocyte and fibroblast gene expression in skin and keloid scar tissue based on deviation analysis of dynamic capabilities. Exp Ther Med 2016; 12: 3633-3641.
[38] Yan M, Song M, Bai R, Cheng S and Yan W. Identification of potential therapeutic targets for colorectal cancer by bioinformatics analysis. Oncol Lett 2016; 12: 5092-5098.
[39] Zhang H, Yu Z, He J, Hua B and Zhang G. Identification of the molecular mechanisms underlying dilated cardiomyopathy via bioinformatic analysis of gene expression profiles. Exp Ther Med 2017; 13: 273-279.
[40] Qiao A, Zhao Z, Zhang H, Sun Z and Cui X. Gene expression profiling reveals genes and transcription factors associated with dilated and ischemic cardiomyopathies. Pathol Res Pract 2017; 213: 548-557.
[41] Kim BY, Song KH, Lim CY and Cho SI. Therapeutic properties of Scutellaria baicalensis in db/db mice evaluated using connectivity map and network pharmacology. Sci Rep 2017; 7: 41711.
[42] Yang H, Shang D, Xu Y, Zhang C, Feng L, Sun Z, Shi X, Zhang Y, Han J, Su F, Li C and Li X. The LncRNA connectivity map: using LncRNA signatures to connect small molecules, LncRNAs, and diseases. Sci Rep 2017; 7: 6655.
[43] Liu X, Zeng P, Cui Q and Zhou Y. Comparative analysis of genes frequently regulated by drugs based on connectivity map transcriptome data. PLoS One 2017; 12: e0179037.
[44] Wang Z, Jiang W, Zhang Z, Qian M and Du B. Nitidine chloride inhibits LPS-induced inflammatory cytokines production via MAPK and NF-kappaB pathway in RAW 264.7 cells. J Ethnopharmacol 2012; 144: 145-150.
[45] Liu Q, Wang T, Zhou L, Song F, Qin A, Feng HT, Lin XX, Lin Z, Yuan JB, Tickner J, Liu HG, Zheng MH, Xu J and Zhao JM. Nitidine chloride prevents OVX-induced bone loss via suppressing NFATc1-mediated osteoclast differentiation. Sci Rep 2016; 6: 36662.
[46] Chen J, Wang J, Lin L, He L, Wu Y, Zhang L, Yi Z, Chen Y, Pang X and Liu M. Inhibition of STAT3 signaling pathway by nitidine chloride suppressed the angiogenesis and growth of human gastric cancer. Mol Cancer Ther 2012; 11: 277-287.
[47] Yuan P, Zheng X, Li M, Ke Y, Fu Y, Zhang Q, Wang X and Feng W. Two sulfur glycoside compounds isolated from lepidium apetalum willd protect NRK52e cells against hypertonic-induced adhesion and inflammation by suppressing the MAPK signaling pathway and RAAS. Molecules 2017; 22.
[48] Su G, Sun G, Liu H, Shu L, Zhang J, Guo L, Huang C and Xu J. Niacin suppresses progression of atherosclerosis by inhibiting vascular inflammation and apoptosis of vascular smooth muscle cells. Med Sci Monit 2015; 21: 4081-4089.
[49] Su S, Duan J, Chen T, Huang X, Shang E, Yu L, Wei K, Zhu Y, Guo J, Guo S, Liu P, Qian D and Tang Y. Corrigendum: frankincense and myrrh suppress inflammation via regulation of the metabolic profiling and the MAPK signaling pathway. Sci Rep 2015; 5: 15597.
[50] Bai D, Cong S and Zhu LP. Attenuation of focal adhesion kinase reduces lipopolysaccharide-induced inflammation injury through inactivation of the wnt and NF-kappaB pathways in A549 cells. Biochemistry (Mosc) 2017; 82: 446-453.
[51] Lu K, Liu G, Yang L, Liu F, Gao L, Shi J, Deng X, Li Q, Xu D and Shi S. Sustainable inflammation transforms hepatic cells by causing oxidative stress injury and potential epithelial-mesenchymal transition. Int J Oncol 2016; 49: 971-980.
[52] Yang D, Jin M, Bai C, Zhou J and Shen Y. Peroxiredoxin 6 suppresses Muc5ac overproduction in LPS-induced airway inflammation through H2O2-EGFR-MAPK signaling pathway. Respir Physiol Neurobiol 2017; 236: 84-90.
[53] Dumka VK, Tandan SK, Raviprakash V and Tripathi HC. Central noradrenergic and cholinergic modulation of formaldehyde-induced pedal inflammation and nociception in rats. Indian J Physiol Pharmacol 1996; 40: 41-46.
[54] Nordling L, Lundeberg T, Ekman P, Liedberg H and Theodorsson E. Role of the autonomic nervous system in catheter-induced urethral inflammation. Eur Urol 1992; 21: 328-331.
[55] Hopkins RW and Damewood CA. Septic shock: hemodynamics of endotoxin and inflammation. Am J Surg 1974; 127: 476-483.
[56] Movva R, Lobb M, P OC, Florin TH, Duley JA and Oancea I. Microbial metabolism of thiopurines: a method to measure thioguanine nucleotides. J Microbiol Methods 2016; 128: 102-107.
[57] Heo J, Wey M and Hong I. Insight into the 6-thiopurine-mediated termination of the invasive motility of tumor cells derived from inflammatory breast cancer. Biochemistry 2011; 50: 5731-5742.
[58] Zhao L, Cen F, Tian F, Li MJ, Zhang Q, Shen HY, Shen XC, Zhou MM and Du J. Combination treatment with quercetin and resveratrol attenuates high fat diet-induced obesity and associated inflammation in rats via the AMPKalpha1/SIRT1 signaling pathway. Exp Ther Med 2017; 14: 5942-5948.
[59] Chen J, Cao X, Cui Y, Zeng G, Chen J and Zhang G. Resveratrol alleviates lysophosphatidylcholine-induced damage and inflammation in vas-

cular endothelial cells. Mol Med Rep 2018; 17: 4011-4018
[60] Zhou ZX, Mou SF, Chen XQ, Gong LL and Ge WS. Anti-inflammatory activity of resveratrol prevents inflammation by inhibiting NFkappaB in animal models of acute pharyngitis. Mol Med Rep 2018; 17: 1269-1274.
[61] Xu Y, Zhang B, Xie D, Hu Y, Li HL, Zhong LL, Wang HW, Jiang W, Ke ZP and Zheng DH. Nanoparticle-mediated dual delivery of resveratrol and DAP5 ameliorates kidney ischemia/reperfusion injury by inhibiting cell apoptosis and inflammation. Oncotarget 2017; 8: 39547-39558.
[62] Wang G, Hu Z, Fu Q, Song X, Cui Q, Jia R, Zou Y, He C, Li L and Yin Z. Resveratrol mitigates lipopolysaccharide-mediated acute inflammation in rats by inhibiting the TLR4/NF-kappaBp65/MAPKs signaling cascade. Sci Rep 2017; 7: 45006.
[63] Alvarenga EM, Souza LK, Araujo TS, Nogueira KM, Sousa FB, Araujo AR, Martins CS, Pacifico DM, de CBGA, Souza EP, Sousa DP and Medeiros JV. Carvacrol reduces irinotecan-induced intestinal mucositis through inhibition of inflammation and oxidative damage via TRPA1 receptor activation. Chem Biol Interact 2016; 260: 129-140.
[64] Formica V, Luccchetti J, Cunningham D, Smyth EC, Ferroni P, Nardecchia A, Tesauro M, Cereda V, Guadagni F and Roselli M. Systemic inflammation, as measured by the neutrophil/lymphocyte ratio, may have differential prognostic impact before and during treatment with fluorouracil, irinotecan and bevacizumab in metastatic colorectal cancer patients. Med Oncol 2014; 31: 166.
[65] Park CH, Hixon DL, Ferguson CB, Hall SL, Risheim CC and Cook CB. Rapid recovery of mycobacteria from clinical specimens using automated radiometric technic. Am J Clin Pathol 1984; 81: 341-345.